Astron. Astrophys. 331, 317–327 (1998)

ASTRONOMY AND ASTROPHYSICS

Excitation of far-infrared lines of OH and maser pumping efficiency in circumstellar envelopes

Thai-Q-Tung[1]⋆, Dinh-V-Trung[1], Nguyen-Q-Rieu[1], V. Bujarrabal[2], T. Le Bertre[1], and E. Gérard[3]

[1] Observatoire de Paris, DEMIRM, 61 Avenue de l'Observatoire, F-75014 Paris, France
[2] Centro Astronómico de Yebes (IGN), Apartado 148, E-19080 Guadalajara, Spain
[3] Observatoire de Paris-Meudon, Arpèges, Place J. Janssen, F-92195 Meudon Cedex, France

Received 28 July 1997 / Accepted 7 October 1997

Abstract. We present the results obtained with a radiative transfer model to investigate the excitation of OH molecules. Fluxes of far-infrared rotational lines of OH are calculated in terms of a radiatively excited envelope and of a radiative transfer model including collisional and radiative excitation. The agreement with the OH far-infrared lines observed with ISO is satisfactory. The 34.6 μm line is found to be in absorption as observed. We also predict that the 53.3 μm line should be seen in absorption and also contributes to the maser pumping process. Maser pumping efficiencies are estimated from the model and compared to the values determined from recent OH far-infrared observations with ISO and OH maser data.

Key words: masers – radiative transfer – stars: circumstellar matter – stars: individual: IRC+10420

1. Introduction

The OH ground state maser lines have been studied extensively since their first detection by Weaver et al. (1965). These maser lines were detected in both interstellar medium and the circumstellar envelope of late type stars. The gross feature of the pumping mechanism of the 1612 MHz maser line is now rather well understood (Elitzur et al. 1978). The absorption of far-infrared (FIR) photons at 34.6 μm and 53.3 μm excites the OH molecules from the $\Pi_{3/2}$ ground state to the $\Pi_{1/2}$ ladder and subsequent cascading downward inverts the populations of the ground state $\Lambda-$doubling levels (Fig. 1). But due to the atmospheric absorption in the FIR region, OH-FIR rotational lines are inaccessible from the ground and the pumping scheme could only be checked indirectly using the infrared continuum flux extrapolated to 34.6 μm. It was shown that there are enough FIR photons to pump the 1612 MHz satellite maser (Evans & Beckwith 1977; Nguyen-Q-Rieu et al. 1979; Epchtein et al. 1980). Recently, Skinner et al. (1997) and Sylvester et al. (1997) reported the first direct detection of the 34.6 μm OH absorption lines in the megamaser galaxy Arp 220 and in the circumstellar envelope of the supergiant star IRC+10420, respectively. In the latter source Sylvester et al. (1997) detected several other OH-FIR lines.

Theoretical works on OH masers have so far concentrated either on multi-level models using a simplified treatment (LVG approximation) of the radiative transfer (Elitzur et al. 1978, Bujarrabal et al. 1980) or on an exact solution for the radiative transfer equation in a two-level maser (Alcock & Ross 1985, Spaans & van Langevelde 1992). Because the maser emission depends critically on the pumping rates (or the pumping conditions) throughout the envelope, a correct treatment of both pumping conditions and maser radiative transfer is required. Collison & Nedoluha (1995) made an attempt to improve the treatment of the radiative transfer in the maser transitions.

In this paper we present a detailed modeling of both pumping conditions and maser radiative transfer calculations in the circumstellar envelope. We apply our model to the case of the supergiant star IRC+10420 where OH-FIR lines have been detected by ISO. Maser pumping efficiencies are calculated and compared to those obtained from the observations.

2. Radiative excitation of OH-FIR lines

We first examine a simple radiative pumping scheme of the OH-FIR lines by photons emitted by the circumstellar dust grains. Fig. 1 shows the six lowest OH rotational states. OH molecules pumped to the $\Pi_{1/2}$(J = 5/2) level by the absorption of 34.6 μm photons return to the ground $\Pi_{3/2}$(J = 3/2) state through the cascades in the $\Pi_{1/2}$ and $\Pi_{3/2}$ ladders to invert the populations of the ground state hyperfine levels. The populations of the upper levels are assumed to be negligible. In this case the FIR rotational line fluxes can be easily calculated by considering the routes downward through various rotational states. A 34.6 μm photon can give rise to 3 photons at 115.2 μm, 98.7 μm and 48.8 μm and the conservation of the number of absorbed photons can

Send offprint requests to: Dinh-V-Trung
⋆ *on leave from Institute of Laser Technology, Hanoi, Vietnam*

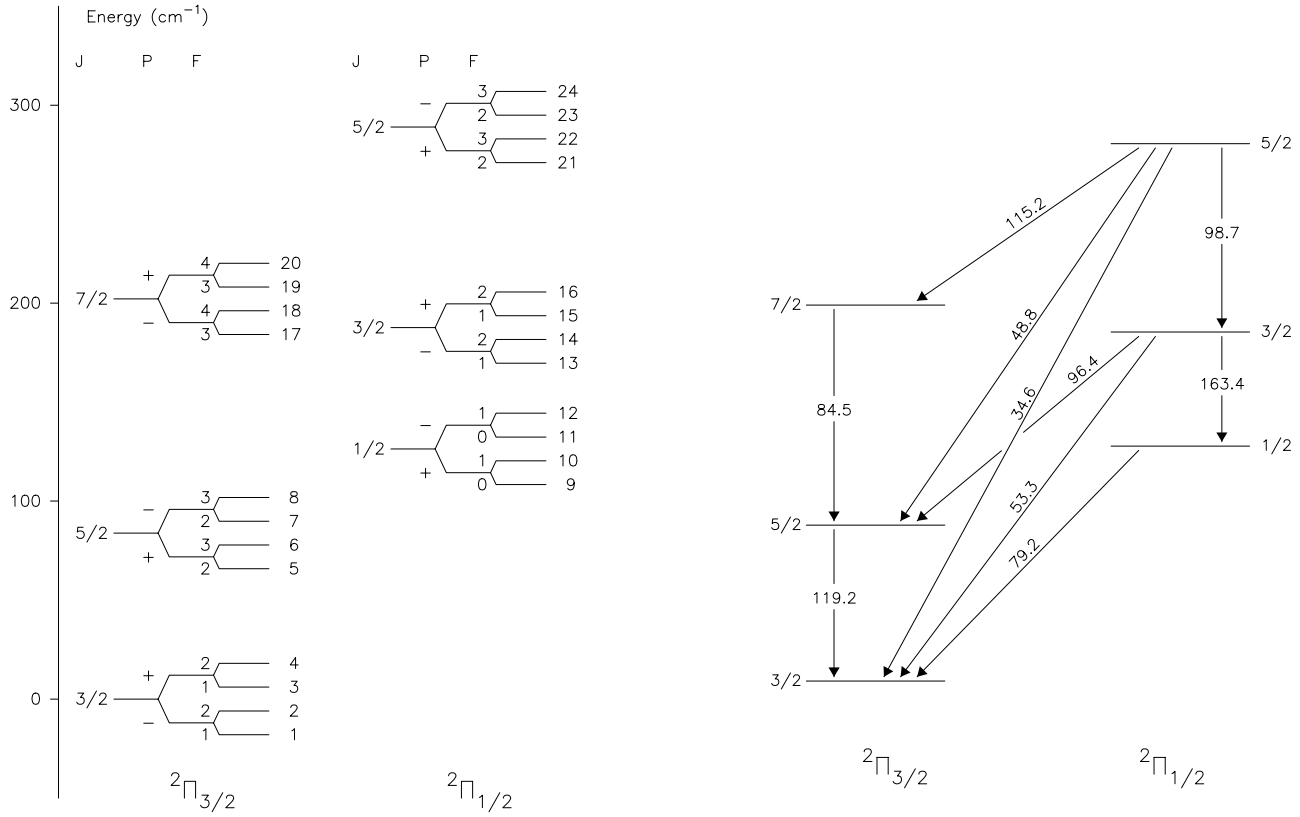

Fig. 1. OH energy level and FIR transition diagram.

be expressed as follows:

$$F_{34.6\mu m} \cdot 34.6 + F_{48.8\mu m} \cdot 48.8 + F_{115.2\mu m} \cdot 115.2 + F_{98.7\mu m} \cdot 98.7 = 0 \quad (1)$$

We use the usual convention of line flux (negative value for absorption). The emission lines are optically thin, as a result, the number of photons emitted is proportional to the line strength.

$$\begin{aligned} F_{98.7\mu m} &= -F_{34.6\mu m} \cdot 34.6/98.7 \cdot C_1 \\ F_{48.8\mu m} &= -F_{34.6\mu m} \cdot 34.6/48.8 \cdot C_1^{'} \\ F_{115.2\mu m} &= -F_{34.6\mu m} \cdot 34.6/115.2 \cdot C_1^{"} \end{aligned} \quad (2)$$

where C_1, $C_1^{'}$ and $C_1^{"}$ are the branching ratios:

$$\begin{aligned} C_1 &= A_{98.7}/(A_{115.2} + A_{98.7} + A_{48.8}) = 0.86 \\ C_1^{'} &= A_{48.8}/(A_{115.2} + A_{98.7} + A_{48.8}) = 0.13 \\ C_1^{"} &= A_{115.2}/(A_{115.2} + A_{98.7} + A_{48.8}) = 0.007 \end{aligned} \quad (3)$$

$A_{115.2}$, $A_{98.7}$ and $A_{48.8}$ are the transition probabilities. The flux of the 84.5 μm line is directly related to the flux of the 115.2 μm line because of the conservation of the number of photons:

$$F_{84.5\mu m} = F_{115.2\mu m} \cdot 115.2/84.5 \quad (4)$$

The photons absorbed or emitted at 53.3 μm alter the intensities of the 163.4 μm and 79.2 μm lines.

$$\begin{aligned} F_{163.4\mu m} &= (F_{98.7\mu m} \cdot 98.7 - F_{53.3\mu m} \cdot 53.3) \cdot C_2/163.4 \\ F_{96.4\mu m} &= F_{163.4\mu m} \cdot 163.4 \cdot (1 - C_2)/C_2/96.4 \end{aligned} \quad (5)$$

where C_2 is the branching ratio of the 163.4 μm transition $C_2 = A_{163.4}/(A_{96.4} + A_{163.4}) = 0.88$

Similarly, the fluxes of the 79.2 μm and the 119.2 μm lines are calculated as follows

$$F_{79.2\mu m} = F_{163.4\mu m} \cdot 163.4/79.2 \quad (6)$$

$$F_{119.2\mu m} = F_{84.5\mu m} \cdot 84.5/119.2 + F_{48.8\mu m} \cdot 48.8/119.2 + F_{96.4\mu m} \cdot 96.4/119.2 \quad (7)$$

If the fluxes of the 34.6 μm absorption line and the 53.3 μm line are known, we can derive all the other FIR lines in the pumping cycle of the OH maser, by using formulae 2-7.

3. The radiative transfer model

In order to investigate both the radiative and collisional processes we need a more elaborate model. The circumstellar envelope is assumed to be spherical. We use the LVG approximation to treat the radiative transfer in the FIR rotational lines. Since the maser lines are very sensitive to the physical conditions in the circumstellar envelope a non-local treatment is used for maser lines in the ground state. Collisional rates between OH and H_2 are taken from Offer et al. (1994). The ratio of ortho-H_2 to para-H_2 is assumed to be equal to 3. Line transition probabilities are taken from Burdyuzha & Varshalovich (1973) and Destombes et al.(1977).

The radiation field consists of the cosmic background radiation with a temperature T_{BG} = 2.7K and of the intensity of FIR emission due to dust grains which are assumed to be optically thin. The dust absorption coefficient may be written as follows:

$$k_d = n_d \cdot \sigma \cdot Q_{abs}(\nu) \tag{8}$$

where n_d, σ and Q_{abs} are the density, cross section ($\sigma = \pi a^2$) and the absorption efficiency of the grain, respectively. In this paper we take $Q_{abs}(\nu) = Q_o \cdot (\nu/\nu_o)^{-p}$, Q_o and ν_o are the absorption efficiency and frequency at $20\mu m$ and p may vary between 1 - 2. The ratio $n_d \cdot \sigma / n_{H_2}$ is adjusted to fit the observed FIR continuum emission of the envelope. The expansion velocity as a function of radius in the envelope is very uncertain. We take the velocity expansion law suggested by Deguchi & Nguyen-Q-Rieu (1990):

$$V(r) = V_\infty \cdot (1 - 3 \cdot R_*/r)^{0.5} \tag{9}$$

where V_∞ is the terminal velocity and R_* is the radius of the central star. The velocity gradient decreases with radius. The value of the velocity gradient ϵ = dlnV/dln r is set to 0.01 when it becomes smaller than 0.01. The exact value of the velocity gradient should have only a minor effect on the final results at least for FIR rotational lines.

The populations of OH molecules are calculated by solving the equations of statistical equilibrium at each grid point. Our formulation of the overlap effect is similar to that presented by Bujarrabal et al. (1980) and by Collison & Nedoluha (1993). The rate equations in the LVG approximation can be written in the form:

$$\begin{aligned}\frac{dn_k}{dt} &= \sum_{j>k} \frac{g_j}{g_k} A_{jk}[\beta_{jk}(n_j - \frac{n_k - n_j}{exp(h\nu_{jk}/k_B T_{BG}) - 1}) \\ &\quad - D_{jk}(n_k - n_j)] + C_{jk}\frac{g_j}{g_k}[n_j - n_k exp(-\frac{h\nu_{jk}}{k_B T_K})] \\ &\quad - \sum_{j<k} A_{kj}[\beta_{kj}(n_k - \frac{n_j - n_k}{exp(h\nu_{kj}/k_B T_{BG}) - 1}) \\ &\quad - D_{kj}(n_j - n_k)] + C_{kj}[n_k - n_j exp(-\frac{h\nu_{kj}}{k_B T_K})] \end{aligned} \tag{10}$$

where n_k is the population of magnetic sublevels, g_k is the statistical weight of the hyperfine level, C_{jk} is the deexcitation rate between levels j and k, T_K is the gas temperature and β_{jk} is the escape probability for the transition j $\rightarrow$ k

$$\begin{aligned}\beta_{jk} &= \frac{1}{2}\int_{-1}^{1} \beta_{jk}(r,\mu) d\mu \\ &= \frac{1}{2}\int_{-1}^{1} \frac{1 - exp[-\tau_{jk}(r,\mu)]}{\tau_{jk}(r,\mu)} d\mu \end{aligned} \tag{11}$$

where $\tau_{jk}(r,\mu)$ is the optical depth in the direction which makes an angle θ with the radius vector r, μ = cos θ and D_{jk} (see Fig. 16) is given by:

$$D_{jk} = (\frac{c^2}{2h\nu_{jk}^3})\frac{1}{2}\int_{-1}^{1} d\mu \beta_{jk}(r,\mu) \int_0^\infty S_{jk}(r')ds \tag{12}$$

The term D_{jk} includes the contribution of the thermal emission from dust grains and of the overlapping lines if line overlap occurs. The integral involving S_{jk}(r') is evaluated along a ray of angle θ.

$$\begin{aligned}\int_0^\infty S_{jk}(r')ds &= \int_0^{s_1} S_{jk}^{dust}(r')ds + \\ &\quad + S_{lm}^{line}(s_1)(1 - exp[-\tau_{lm}(s_1,\mu')]) + \\ &\quad + exp[-\tau_{lm}(s_1,\mu')]\int_{s_1}^\infty S_{jk}^{dust}(r')ds \end{aligned} \tag{13}$$

where S is the source function:

$$S_{jk}^{dust} = \frac{2h\nu_{jk}^3}{c^2}\frac{\pi a^2 Q_{abs}(\nu_{jk}) n_d}{exp(h\nu_{jk}/k_B T_D) - 1} \tag{14}$$

T_D is the dust temperature and

$$S_{lm}^{line} = \frac{2h\nu_{lm}^3}{c^2}\frac{n_l}{n_m - n_l} \tag{15}$$

$\tau_{lm}(s_1,\mu)$ is the optical depth of the l $\rightarrow$ m line which overlaps the j $\rightarrow$ k line in the direction μ. The optical depth τ_{lm} and the source function S_{lm} of the overlapping line l $\rightarrow$ m are evaluated exactly at the position s_1 where this line is redshifted by the velocity shift $\Delta V_{lm,jk}$ between the two lines. The term D_{jk} can be easily generalized in the case of multiple overlaps. As pointed out by Collison & Nedoluha (1995), using the LVG approximation to calculate the FIR average intensity usually gives good results in comparison with direct calculations. The solution for the level populations is obtained by iterating between a calculation of the term D_{jk} at all grid points and a calculation of the populations throughout the OH shell. By doing this we have explicitly taken into account the variation of physical conditions in the envelope. The emergent profiles of OH-FIR rotational lines are then calculated from the populations in the envelope. The intensity along a line of sight with an impact parameter p directed from the observer toward the envelope is given by:

$$\begin{aligned}I_p(\nu) &= \int_{-\infty}^{z_1} S_\nu^{dust} dz + S_{jk}(1 - e^{-\tau_{jk}}) \\ &\quad + e^{-\tau_{jk}}[\int_{z_1}^{z_2} S_\nu^{dust} dz + S_{lm}(1 - e^{-\tau_{lm}}) \\ &\quad + e^{-\tau_{lm}}\int_{z_2}^\infty S_\nu^{dust} dz] \end{aligned} \tag{16}$$

z_1, z_2 are the positions in the envelope where photons of the j $\rightarrow$ k and l $\rightarrow$ m lines are emitted. This formula can be easily generalized in the case of multiple overlaps. The profile observed by an observer at a distance D to the source is then calculated:

$$F(\nu) = [\int_0^\infty I_p(\nu) 2\pi p dp]/D^2 \tag{17}$$

The LVG approach simplifies enormously the radiative transfer problem and allows us to calculate quickly the OH populations over the whole envelope and to derive various observable quantities. But this formalism may lead to significant errors since

the expansion velocity in the envelope is nearly constant implying the interaction of different parts of the shell. This situation may have great effect on the population inversion of the ground state OH masers. Following Collison & Nedoluha (1995), we use a model in which the radiative transfer equations of the 4 ground state maser transitions are solved non-locally while all other transitions (FIR hyperfine lines and microwave lines in the upper states) are treated under the LVG formalism. The populations from the LVG model described above are used as an input to the calculations of the populations of the maser levels. More details can be found in Appendix A and in the paper of Collison & Nedoluha (1995). Once the overall populations at all grid points are obtained, the maser profiles and luminosities can be calculated.

4. Application to IRC+10420. OH-FIR lines

The supergiant star IRC+10420 has a large FIR excess which is attributed to the presence of a cold circumstellar dust shell. In addition to strong OH main line masers and satellite masers, several OH-FIR rotational lines have been detected with the ISO spectrometers by Sylvester et al. (1997) (Table 1). The mass loss rate is still uncertain but from recent observations of Oudmaijer et al. (1996) it must be at least equal to 10^{-4} $M_{\odot}yr^{-1}$. The distance to this star is also uncertain ranging from 3 - 5 kpc; we adopt the value of 3.4 kpc determined by Mutel et al. (1979).

4.1. Infrared continuum emission

IRC+10420 is known to vary irregularly. We adopted the spectrum as synthesized by Hrivnak et al. (1989). In Fig. 2, the dots represent the ground-based data and the triangles, the IRAS data as color-corrected by these authors. Using an existing model of radiative transfer through a spherical circumstellar dust shell (Le Bertre et al. 1984), we have attempted to fit this spectrum. The dust is taken to be of the "dirty silicate" type (Jones & Merrill 1976). The central star has been assumed to radiate as a blackbody at 6100 K on the basis of its spectral type: "F8Ia, or perhaps Iab" (Giguere et al. 1976).

One of our best fits is displayed in Fig. 2. together with the near and FIR photometric data. The temperature of the hottest grains has been set to 650 K and the optical depth at 10 μm, $\tau_{10\mu m}$, to 1.0. The dust density distribution has been taken to vary as $\propto 1/r^2$. The quality of the fit is comparable to that of the fits already obtained by Hrivnak et al. (1989) or Oudmaijer et al. (1996). In general, it is difficult to adjust the optical and near-infrared parts of the spectrum. In fact, the shape of the energy distribution is similar to those of bipolar objects such as AFGL 2688 or the Red Rectangle. As shown by Lopez et al. (1997), their spectra can be better modeled with an axisymmetrical dust shell. There are evidences (e.g. Diamond et al. 1983) that IRC +10420 is a bipolar source and that the line of sight is near its equatorial plane as for the objects discussed by Lopez et al. (1997).

On the basis of such fit and the adopted distance of 3.4 kpc, the bolometric luminosity is estimated to be $\sim 3.7\ 10^5\ L_{\odot}$. This is slightly superior to the luminosity of F8 hypergiants (Lang 1991). However, our estimation may be biased by the assumption of spherical symmetry. Using the relation (2b) of Le Sidaner & Le Bertre (1993), the dust mass loss rate is found to be $\sim 3\ 10^{-6}\ M_{\odot}\ yr^{-1}$. For a gas-to-dust mass ratio in the range 100-200, this translates to a total mass loss rate of 3-6 $10^{-4}\ M_{\odot}\ yr^{-1}$. In the following, we will adopt $5\ 10^{-4}\ M_{\odot}\ yr^{-1}$ in good agreement with the estimation of Oudmaijer et al. (1996).

The fit in the far-infrared ($\lambda \geq 20\mu$m), is not of a sufficient quality for the modeling of the OH lines. Therefore, we have interpolated the IRAS data by using the optically thin model presented in Sect. 3. In this model, the dependence of dust absorption efficiency on frequency is assumed to be a power law similar to that used in Volk & Kwok (1988):
p = 1 for $\lambda \leq 84\ \mu$m
p = 2 for $\lambda > 84\ \mu$m.

The variation of temperature of dust grains with radius which fits IRAS observations for $\lambda > 20\ \mu$m is:

$T_D(r) = T_{Dmin} \cdot (R_{Dmin}/r)^{0.4}$

where R_{Dmin} is the inner boundary of the dust shell: R_{Dmin} = $8.5\ 10^{15}$ cm and T_{Dmin} = 475 K. The outer radius of the dust envelope R_{Dmax} is defined as the radius beyond which the dust FIR flux in our computation does not change. In our model R_{Dmax} is found to be 10^{18} cm (T_D at this radius is about 70 K).

The output continuum spectrum is displayed in Fig. 2.

4.2. Radiative excitation in an optically thin envelope

We have applied the radiative pumping model described in Sect. 2 to the FIR rotational lines of OH recently observed by ISO. All line fluxes are derived from the fluxes of the pumping absorption lines at 34.6 μm and 53.3 μm. The 34.6 μm line was detected in IRC+10420 by ISO but not the 53.3 μm line. We take the upper limit of the 53.3 μm line flux from the ISO observations as the flux of the 53.3 μm absorption line. The results given in Table 1 show that the FIR line intensities predicted by the optically thin radiative model tend to be systematically weaker than the observed intensities. Radiative pumping alone seems insufficient to account for the OH-FIR lines in the envelope of IRC+10420. Both the collisional excitation and the radiative trapping must play an important role in the excitation of OH molecules.

4.3. Collisional and radiative excitation of OH

We use the model described in Sect. 3 which includes both the collisional and the radiative excitation. The mass loss rate and the terminal velocity are taken to be $5\ 10^{-4}$ $M_{\odot}yr^{-1}$ and 35 kms^{-1} respectively.

The limits of the OH shell are estimated from the VLA observations of Nedoluha & Bower (1992):
$R_{OHmin} = 2\ 10^{16}$ cm and $R_{OHmax} = 10^{17}$ cm. The dependence of the gas temperature on radius is highly uncertain but we found from our model that the gas temperature has a small effect on the excitation of OH-FIR lines. We have chosen:

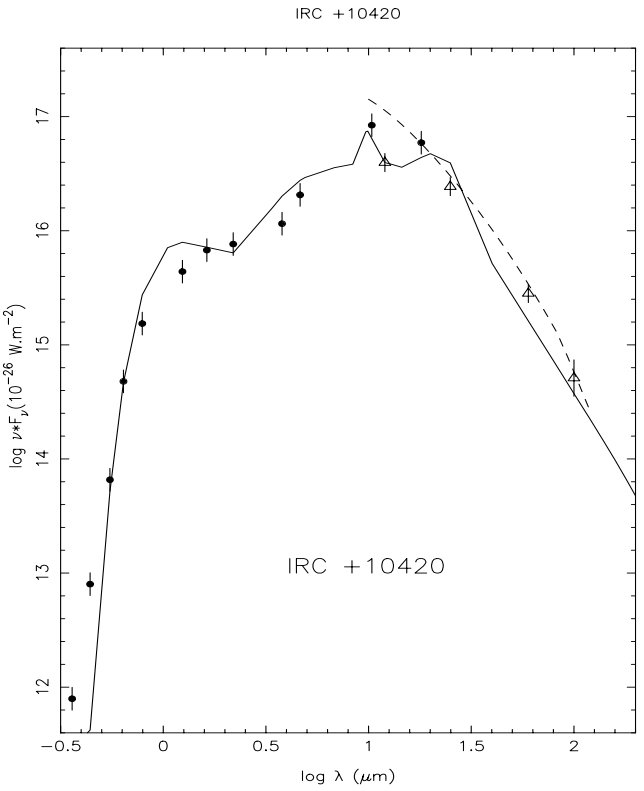

Fig. 2. The spectral energy distribution of IRC +10420; the dots represent ground-based data synthesized by Hrivnak et al. (1989) and the triangles, IRAS data. The solid line represents a fit with a spherical model of circumstellar dust shell (Sect. 4.1). The dashed line is a fit of the far-infrared spectrum based on an optically thin model (Sect. 3).

$T_g(r) = T_{g0} \cdot (R_{g0}/r)^{0.5}$

T_{g0} is taken to be 100 K at $R_{g0} = 2\ 10^{16}$ cm.

OH molecules are produced in the outer part of the circumstellar envelope due to photodissociation of H_2O by the interstellar UV photons. The contribution of the stellar UV photons is negligible except for the regions very close to the central star. The model of Netzer & Knapp (1987) shows that for a star with a mass loss rate comparable to that of IRC+10420, OH molecules are formed at a radial distance of about 10^{17} cm. This prediction is in rough agreement with VLA observations of Nedoluha & Bower (1992). Because the radial distribution of OH molecules depends on several factors such as the UV field, dust shielding ...etc, we simply assume that OH abundance is constant throughout the OH envelope. The value of OH abundance which fits the ISO observations towards IRC+10420 is $1.2\ 10^{-5}$.

Our model provides a satisfactory fit to the intensities of OH-FIR rotational lines except for the 79.2 μm line which is underestimated by 60 % (Table 1). Our model predicts that the 53.3 μm line which turns out to be also in absorption can be a pumping line. A sample of the calculated rotational line profiles is shown in Fig. 3-6. We present only one of the two Λ-doubling profiles since they have about the same profile. Because the spectrometers on board of the ISO satellite have spectral elements much larger than the OH-FIR linewidth determined by the expansion velocity of the envelope, the observed line profiles are averaged out. As a result, the FIR observed amplitudes appear weaker than the calculated amplitudes.

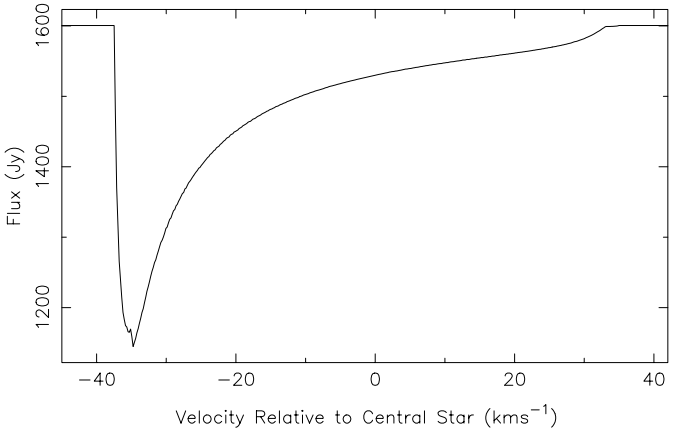

Fig. 3. The calculated 34.6μm Λ-doublet spectrum. The velocity is relative to the central star (V_{LSR} = 75 kms^{-1})

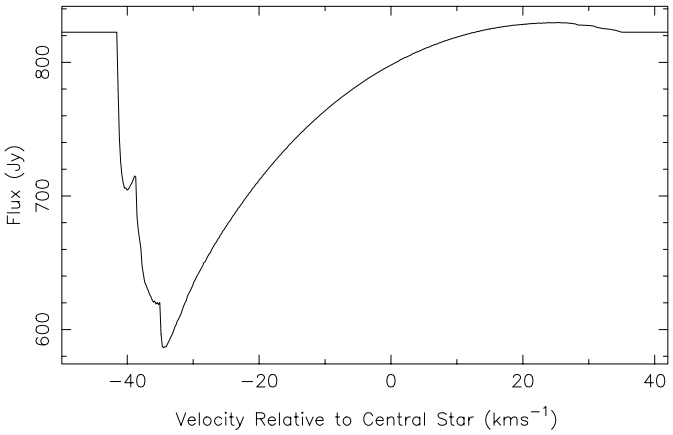

Fig. 4. The calculated 53.3μm Λ-doublet spectrum. Same legend as Fig. 3.

In our model, there is an absorption by OH at zero and positive velocities in the lines at 34.6 μm and 53.3 μm (Fig. 3). This is an indication of the presence of warm dust ($T_D \sim 70$ - 180 K) outside the OH shell. Therefore, this spectral feature could be used to infer the relative location of the warm dust with respect to the OH envelope. But considering the small amplitude of the absorption and the required high velocity resolution of the observed spectra, this test is probably not feasible with current instruments (i.e ISO).

5. OH maser emission from IRC+10420

5.1. Observations

The observations of OH maser lines from IRC+10420 were carried out with the Nançay radiotelescope on April 16th 1997.

Table 1. OH-FIR line fluxes from observations and models

Wavelength (μm)	Flux (10^{-12} ergs^{-1}cm^{-2})		
	Observation* (November 1996)	Radiative excitation model	LVG model
34.6	-4.8 $\pm$ 0.4	(-4.8)	-5.1
48.8	$<$ 15	0.4	0.15
53.3	$<$ 1.6	(-1.6)	-1.5
79.2	5.2 $\pm$ 0.8	2.5	2.3
84.5	$<$ 1.0	0.01	0.03
96.4	$<$ 0.3	0.3	0.6
98.7	2.6 $\pm$ 0.2	1.4	1.7
119.2	0.75 $\pm$ 0.05	0.4	0.6
163.4	1.52 $\pm$ 0.07	1.2	1.1

* from Sylvester et al. (1997)

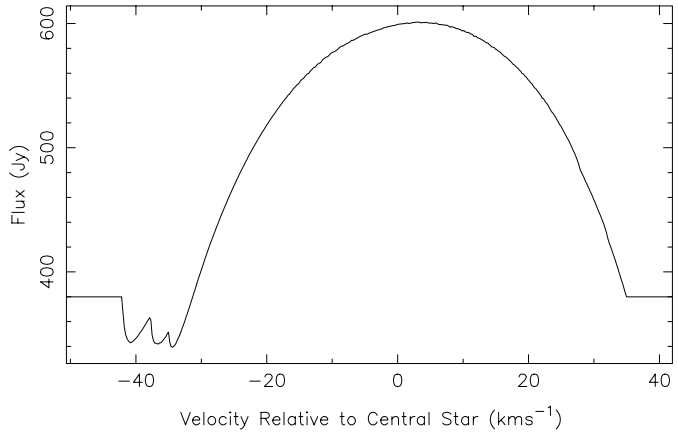

Fig. 5. The calculated 79.2μm Λ-doublet spectrum. Same legend as Fig. 3.

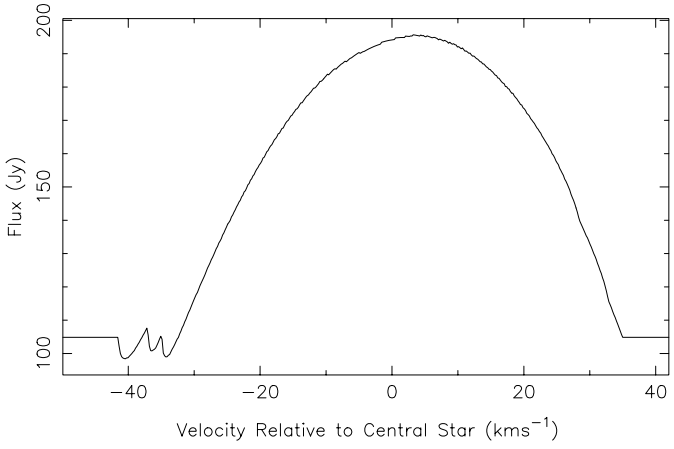

Fig. 6. The calculated 119.2μm Λ-doublet spectrum. Same legend as Fig. 3.

The instrument has a RAxDec beam of 3.5' x 19'. The system noise temperature was 45 K; the antenna temperatures were converted to flux densities using the efficiency curve of the radio telescope which is 0.9 K/Jy for point sources at zero declination. An autocorrelation spectrometer consisting of 4 banks of 256 channels with 0.57 kms^{-1} resolution was used to observe the 1612 MHz, 1665 MHz and 1667 MHz lines in both left and right circular polarizations. The observations were made in the frequency-switching mode with a total velocity coverage of 146 kms^{-1}. The spectra shown on Figs. 7-9 have been Hanning smoothed and the final resolution is 1.14 kms^{-1}. The rms noise level is 0.1 Jy. One may argue that the OH radio and FIR line observations are not contemporaneous. However, the 1612 MHz OH emission of IRC+10420 is regularly monitored at Nançay and the last profile was taken on 12 October 1996 at about the same periods as the ISO observations. Within calibration uncertainties ($\simeq$ 10%), there is no evidence for a significant flux variation over a 6 month period, at least at 1612 MHz.

5.2. Model calculations

The absorption of 34.6 μm and 53.3 μm photons leads to the inversion of the 1612 MHz transition. A consequence of this pumping cycle is that the other satellite line at 1720 MHz is anti-inverted. The occurrence of main line masers is more difficult to explain. Bujarrabal et al. (1980) proposed the overlap of FIR hyperfine lines of OH as the main mechanism for the inversion of main lines. The 1612 MHz satellite line is also enhanced by the overlap effect. In the model of Bujarrabal et al. (1980) the Doppler shifts are limited to a maximum velocity (2 kms^{-1}). This limit is probably valid for optically thin Mira variables or if OH masers arise from clumps occupying a small fraction of the envelope. But OH-IR objects usually have higher expansion velocity and hence higher velocity limits are expected. These authors also used local physical conditions to evaluate the source function and the optical depth of the FIR overlapping lines, which are spatially separated from the overlap region. In spite of these limitations, the calculations of Bujarrabal et al. (1980) did reveal many important implications of the FIR line overlap on the inversion of OH main line masers.

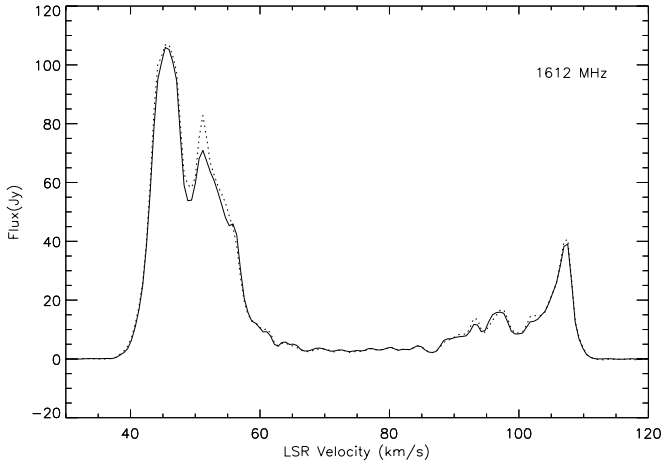

Fig. 7. Line profile of the 1612 MHz maser. Solid line stands for left circular polarization and dotted line for right circular polarization.

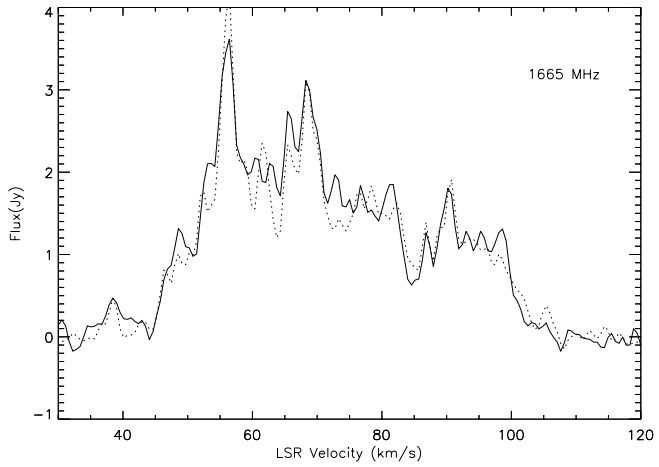

Fig. 8. Line profile of the 1665 MHz main line maser. Same legends as Fig. 7

Recently, Collison & Nedoluha (1993, 1994, 1995) built a more sophisticated model of the circumstellar OH maser taking into account the variation of the physical conditions in the circumstellar envelopes. Their results are qualitatively consistent with those obtained by Bujarrabal et al. (1980), but when the limitation of the Doppler shift was dropped they found that the effect of the FIR hyperfine line overlap was much smaller. They were unable to explain the dominance of main line masers over the satellite maser in the context of their model for the circumstellar envelopes. They proposed the overlap between OH near-infrared (NIR) vibrational line and a water line at 2.8 μm as a possible mechanism to explain the main line masers. Although the NIR overlap seems to be a possible pumping mechanism, so far no attempt has been made to check quantitatively this effect. One major improvement was implemented by Collison & Nedoluha (1995). They solved directly the equation of radiative transfer for maser lines in the envelope instead of relying on the Sobolev assumption.

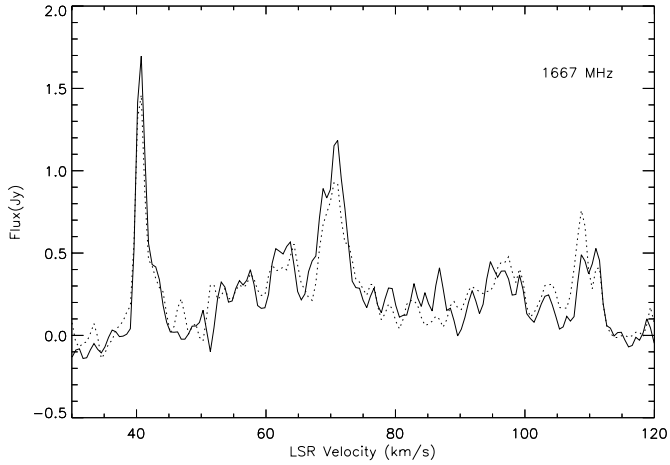

Fig. 9. Line profile of the 1667 MHz main line maser. Same legends as Fig. 7

Using a non-local radiative transfer model with the physical conditions of the envelope which fit the OH rotational line intensities, we obtain solutions for the populations throughout the OH shell in two cases. In model 1 we limit the Doppler shift to 2 kms^{-1} and in model 2 all overlapping hyperfine pairs, which correspond to the expansion velocity (V_{exp} = 35.0 kms^{-1}) of IRC+10420, are included. The local linewidth (FWHM) is assumed to be 1.0 kms^{-1} in the envelope. The emergent OH maser profiles are given in Figs. 12-15. There is a clear tendency for the 1612 MHz satellite maser to dominate the main line masers. This is qualitatively consistent with the observations. Although in model 1 the two main line masers are present, the 1665 MHz maser is however much weaker than the 1667 MHz maser. The observations towards IRC+10420 indicate that the 1665 MHz line is stronger than the 1667 MHz line. As already noted by Collision & Nedoluha (1995) we also find that the main line emission comes from the region which is coincident with the unsaturated core of the 1612 MHz maser. But the behaviour of the main line masers are very different (see Fig. 10). The reason is as follows: the 1667 MHz maser is partially saturated while the 1665 MHz main line is not inverted in the inner and outer parts of the envelope. Therefore in the radial direction, some 1665 MHz maser photons are reabsorbed by OH molecules, thus reducing its intensity. The calculated total flux of the 1667 MHz maser is much greater than that of the 1665 MHz maser. In model 2 when all overlapping pairs are included, the main line emission is quenched while the 1612 MHz satellite maser is strongly enhanced. Model 2 fails to reproduce the OH main line maser emission. See Table 2.

5.3. Maser pumping efficiency

The pumping efficiency of the OH masers is an important parameter to constrain the models. Previous estimates of the pumping efficiency suffered from the absence of FIR line data (Evans & Beckwith 1977; Nguyen -Q-Rieu et al. 1979; Epchtein et al. 1980). They were based on the continuum observations around

Table 2. Calculated and observed fluxes of the OH masers.

Line frequency (MHz)	Total flux (erg cm^{-2}s^{-1}) Model 1 (Doppler shift $\leq$ 2.0 km/s)	Model 2 (Doppler shift $\leq$ 35.0 km/s)	Observations
1612	5.0E-17	1.7E-16	8.2E-17
1665	1.0E-18	-1.4E-22	5.0E-18
1667	1.6E-17	-1.5E-22	1.2E-18

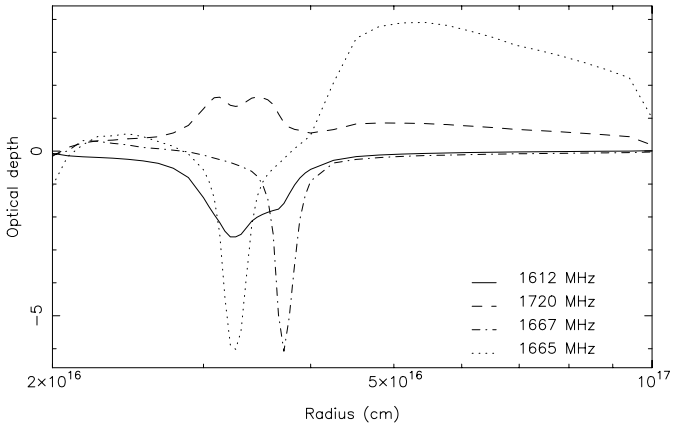

Fig. 10. Optical depth of four ground state transitions in the tangential direction (Eq. A10) with populations derived from non-local calculations in model 1.

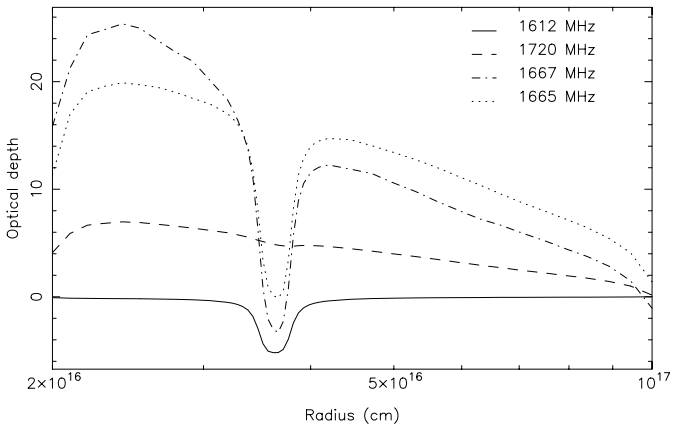

Fig. 11. Optical depth of four ground state transitions in the tangential direction (Eq. A10) with populations derived from non-local calculations in model 2.

30 μm. The detection of the 34.6 μm line by ISO allows us to reconsider this issue. Our model predicts that the 53.3 μm line is also in absorption. As a result, the maser pumping efficiency of the 1612 MHz maser can be defined as the ratio of the number of maser photons to that of FIR photons:

$$\epsilon = \frac{N_{1612MHz}}{N_{34.6\mu m} + N_{53.3\mu m}} \tag{18}$$

The envelope of IRC+10420 is a type II source which emits preferentially the 1612 MHz line. Owing to the uncertainties

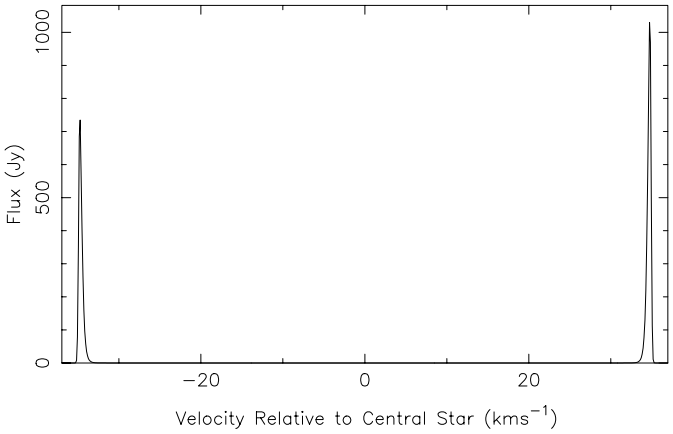

Fig. 12. Line profile of the 1612 MHz maser from model 1.

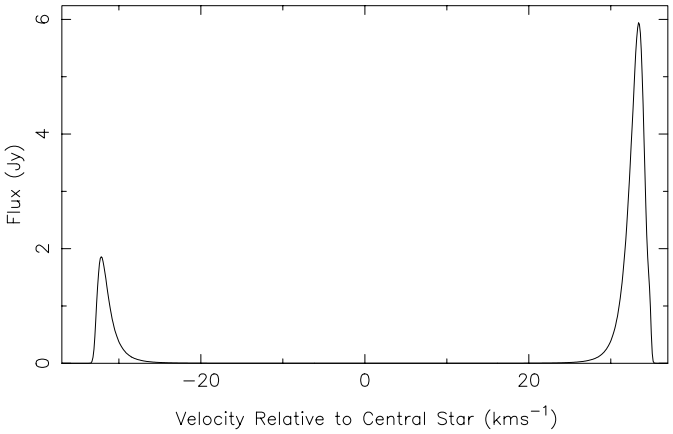

Fig. 13. Line profile of the 1665 MHz maser from model 1.

in the shell parameters, the fluxes determined by our model do not fit closely the observations. The pumping efficiencies for the 1612 MHz maser line estimated from formula (18) are 0.04 in model 1, 0.12 in model 2. Since the 53.3 μm line has not been detected we redefine the observed pumping efficiency as the ratio:

$$\epsilon = \frac{N_{1612MHz}}{N_{34.6\mu m}} \tag{19}$$

The observed pumping efficiency is then equal to 0.09. The corresponding calculated efficiency obtained from model 1 is 0.05. Our calculations also demonstrate that saturated masers convert more efficiently the pumping photons into maser photons than

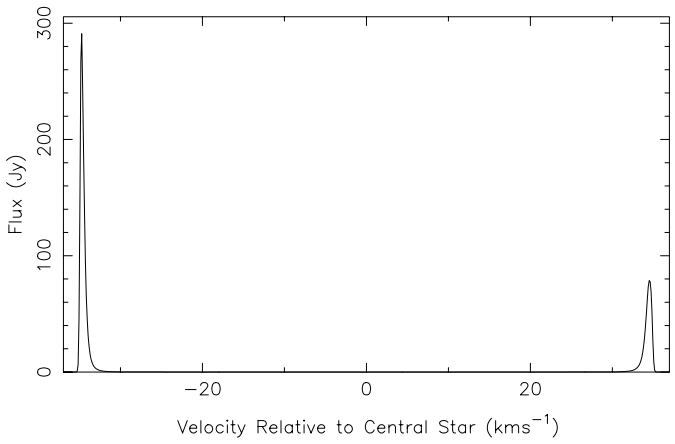

Fig. 14. Line profile of the 1667 MHz maser from model 1.

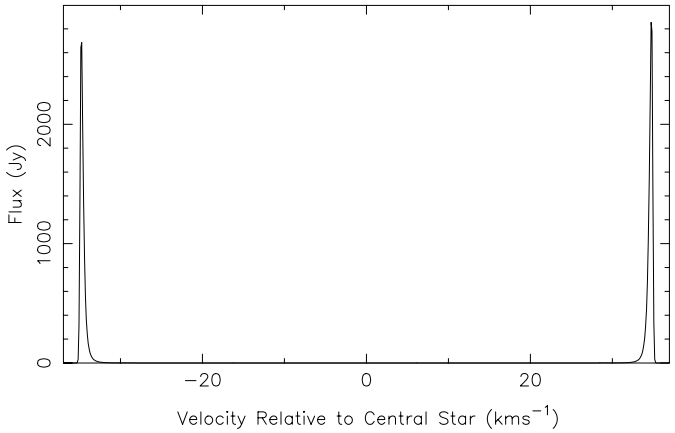

Fig. 15. Line profile of the 1612 MHz maser from model 2.

the non-saturated masers. In model 2 the 1612 MHz maser is strongly saturated, thus the pumping efficiency is much higher (0.17). This characteristic of saturated masers is predicted by Elitzur (1992) using a phenomenological model of two-level maser.

6. Discussion

IRC+10420 is a peculiar star showing large mass loss rate ($5\,10^{-4} M_{\odot}\mathrm{yr}^{-1}$) and high expansion velocity (35 kms^{-1}). In the OH envelope, many complicated physical processes may come into play, for example the turbulence, the non-uniform distribution of OH molecules, the departure from spherical geometry, thus making the modeling of OH maser emission particularly difficult. The striking difference between the observed maser line profiles suggests that they originate from different regions of the envelope, contrary to our models which indicate that the 1612 MHz line and the main lines come from the same region (Fig. 10). The appearance of a middle peak close to the stellar velocity in the observed main line spectra (Fig. 8-9) probably indicates that the OH envelope has multiple shells. The fact that only model 1 produces main line maser emission proves that the standard model of OH main line masers (smooth outflow of material combined with FIR line overlap) is not realistic enough to explain the maser emission of IRC+10420. Recent observations with high angular and spectral resolution by Richards (1997) of water and OH masers from several supergiant stars show that OH masers come from clumps and the distribution of these clumps is not spherical. OH main line masers appear at smaller radii in comparison with the 1612 MHz satellite maser.

In addition, maser profiles calculated from either model 1 or model 2 are too narrow in comparison with observations. The wide maser peak ($\sim$10 kms^{-1}) cannot be explained by increasing the value of the velocity dispersion (σ) in the envelope. Thus a deviation from smooth outflow and a possible NIR pumping mechanism must be considered. Alcock & Ross (1985) propose that mass loss occurs in the form of clumps of material ejected randomly from the central star. As a consequence, the emergent maser profile can be the superposition of the maser emission from individual clumps. Random distribution of clumps results in maser profiles with wide peaks. High sensitivity observations of OH masers and modeling by Zell & Fix (1990) seem to give some support to the clumpiness nature of the circumstellar envelope. On the other hand, clumpiness can also provide a natural explanation to the limit of the Doppler velocity between overlapping lines. This condition is necessary to reproduce main line masers when FIR line overlap is considered. If we assume that radiative interaction between clumps is negligible, FIR line overlap occurs essentially between OH molecules inside the clump. Consequently, the Doppler shift between overlapping lines is limited by the clump size and the expansion velocity. In the envelope of optically thin Mira variables where expansion velocity is small, the FIR overlap is a mechanism capable of producing main line masers and also contributes to the inversion of the satellite maser.

NIR overlap between a NIR H_2O line and OH line at 2.8 μm was first suggested by Cimerman & Scoville (1980) to account for the OH main line emission from circumstellar envelopes. A velocity shift of 11 kms^{-1} between the H_2O-NIR line and the OH-NIR line determined by Cimerman & Scoville (1980) seems unlikely to be realized in many OH maser sources. But recently, Collison & Nedoluha (1994) found another possible overlap between H_2O and OH lines with a velocity shift of only about 6 kms^{-1}. This mechanism may be at work in IRC+10420 due to its high expansion velocity.

Although we have adopted a non-local radiative transfer to treat the OH ground state maser lines, some uncertainties still remain in our model. The pumping conditions in the OH shell are determined using the LVG approximation. The thermal overlap between two close FIR hyperfine lines is not considered in our model. The fact that the Doppler shift between some OH-FIR lines is of only about 0.6 kms^{-1} together with a local linewidth of 1 kms^{-1} would result in a thermal overlap. A correct treatment of this effect will require an intricate direct integration of the radiative transfer equations of all OH-FIR hyperfine and microwave lines. For the moment, non-local FIR line overlap is the simplest way which allows us to determine the pumping conditions of ground state masers in the envelope.

7. Conclusions

We have presented a model to calculate the FIR and maser emission of OH in circumstellar envelopes. We applied our model to the envelope of IRC+10420. Our model provides a satisfactory fit to the FIR observations of ISO. The model with low Doppler shift (model 1) seems to be more appropriate to explain the observed maser data. Even in this case, the maser lines are only fitted qualitatively. The pumping efficiency estimated from our model is of the order of that determined from the observations. The large discrepancy between observations and models of OH maser emission clearly demonstrates the necessity of having detailed knowledge of the parameters such as dust emission, shell geometry, velocity field. Observations with high spatial resolution and careful modeling of OH density distribution are also required to build a complete model of OH emission and to derive the physical conditions in the envelope.

Acknowledgements. We would like to thank the referee Dr. S. Deguchi, whose comments help to improve the paper. Our thanks also go to Dr. Ewine F. van Dishoeck for kindly providing us the OH collisional cross sections.

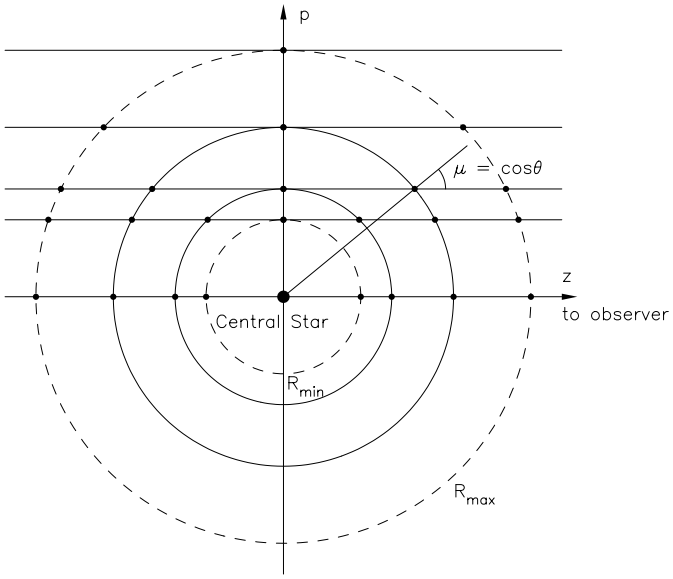

Fig. 16. Radial grid points used to calculate the maser average intensity.

Appendix

The main point of our model is the removal of the Sobolev approximation in solving the radiative transfer equation of maser lines. The maser intensity is the solution of the usual radiative transfer equation:

$$\frac{dI_{jk}(\nu)}{ds} = -k_{jk}(\nu) \cdot I_{jk}(\nu) + \epsilon_{jk}(\nu) \tag{A1}$$

where ϵ_{jk} and k_{jk} are local emission and absorption coefficients, ds is the differential ray path. Complete redistribution is assumed which implies that the absorption and emission line profiles are identical. In that case, the quantity used in the statistical equilibrium equation is the average intensity J_{jk}:

$$J_{jk} = \int \frac{1}{4\pi} \int I_{jk}(\theta,\phi) \cdot \phi_{jk}(\nu) d\nu d\Omega \tag{A2}$$

where the line shape $\phi_{jk}(\nu)$ is assumed to be gaussian with a velocity dispersion σ including thermal width and microturbulence in the envelope ($\phi(\nu) \sim \exp[-(\frac{\nu-\nu_0}{\sigma\cdot\nu_0/c})^2]$, FWHM = $1.67\cdot\sigma$). In order to calculate the average intensity J_{jk} we use the same approach described in the paper of Dickel & Auer (1994). The OH volume is divided into shells with a large number of radial grid points. A set of impact parameters p are chosen tangential to the shells as shown in the Fig. 16. Because the maser emission is essentially beamed into the radial direction, a large number of impact parameters p distributed over the range p = 0 to p = R_{OHmin} are chosen to ensure the correct calculation of the averaged intensity of the maser lines. The radiative transfer equation is solved along the line of sight at each p. The averaged intensity J_{jk} is evaluated by replacing the integral over angle by a weighted sum of I_{jk} for all rays that intersect a shell and a simple integration over frequency. For any maser transition j→k the net rate of molecules going to the lower maser level due to spontaneous and induced emission is :

$$A_{jk} n_j g_j - J_{jk} B_{jk} g_j (n_k - n_j) \tag{A3}$$

or

$$A_{jk} n_j g_j - \tilde{J}_{jk} A_{jk} g_j (n_k - n_j) \tag{A4}$$

where A_{jk} and B_{jk} are the Einstein coefficients and $\tilde{J}_{jk}$ is the reduced intensity:

$$\tilde{J}_{jk} = (\frac{2h\nu_{jk}^3}{c^2})^{-1} \cdot J_{jk} \tag{A5}$$

In the LVG formalism, the mean intensity is expressed directly in term of local escape probability β_{jk} and local source function:

$$\tilde{J}_{jk} = \tilde{S}_{jk}(1 - \beta_{jk}) + \beta_{jk} \tilde{I}_{BG} \tag{A6}$$

with

$$\tilde{S}_{jk} = \frac{n_j}{n_k - n_j} \tag{A7}$$

By inserting the expression (A6) into the expression (A4) we find the usual form of the radiative term in the rate equation (Eq. 10) . In the case of maser lines, the average intensities calculated from Eq. (A2) are coupled to the emission and absorption coefficients in the entire envelope. Because we make use of the Newton-Raphson method to solve the rate equations, explicit derivatives of each term in the rate equation with respect to the local populations are needed. One easy way to do this is to express the average intensity $\tilde{J_{jk}}$ in term of the local escape probability and the local source function:

$$\begin{aligned} \tilde{J_{jk}} &= \gamma_{jk} \cdot \tilde{J}_{jk,LVG}(\alpha) \\ &= \gamma_{jk}[\tilde{S}_{jk}(1 - \beta_{jk}(\alpha)) + \tilde{I}_{BG}\beta_{jk}(\alpha)] \end{aligned} \tag{A8}$$

$\gamma_{jk}(r)$ is a proportional factor introduced to make the correspondence between the exact average intensity and that calculated using the LVG formalism. This substitution ensures that the term in the rate equation which corresponds to the average intensity in each maser line is equal to that calculated exactly by Eq. (A2). The parameter $\alpha_{jk}(r)$ is a modification to the local escape probability

$$\beta_{jk}(r,\alpha) = \frac{1}{2}\int_{-1}^{1} d\mu \frac{1-e^{-\alpha(r)\cdot\tau_{jk}(r,\mu)}}{\alpha(r)\cdot\tau_{jk}(r,\mu)} \quad \text{(A9)}$$

where τ_{jk} is the usual optical depth evaluated using the populations at r. For the tangential direction ($\theta = \frac{\pi}{2}$) the optical depth in the LVG formalism is a good approximation to the real one:

$$\tau_{jk} = \frac{c^3}{8\pi\nu^3}\frac{r}{v}A_{jk}g_j(n_k - n_j) \quad \text{(A10)}$$

This equation is used to present the results of the models. The use of α ($\alpha \leq 1$) in expression (A9) is necessary to prevent numerical overflows in the unsaturated core of OH masers where the population difference is much larger than in the saturated region. The values of α for all maser transitions are fixed in all calculations. A solution for the overall populations in the envelope is obtained by iterating between a calculation of the average intensity in the maser lines and the parameter γ_{jk} at each grid point and a calculation of the populations using the Newton-Raphson method. The convergence is achieved when the parameters γ_{jk} at all grid points change by less than 10^{-3} between two successive iterations .

References

Alcock C., Ross R., 1985, ApJ 305, 837
Bujarrabal V., Guibert J., Nguyen-Q-Rieu, Omont A., 1980, A&A 84, 311
Burdyuzha V.V., Varshalovich D.A. ,1973, AJ 16, 980
Cimerman M., Scoville N., 1980, ApJ 239, 526
Collison A.J., Nedoluha G.E., 1993, ApJ 413, 735
Collison A.J., Nedoluha G.E., 1994, ApJ 422, 193
Collison A.J., Nedoluha G.E., 1995, ApJ 442, 311
Deguchi S., Nguyen-Quang Rieu, 1990, ApJ 360, L27
Destombes J.L., Marliere C., Baudry A., Brillet J., 1977, A&A 60, 55
Diamond P.J., Norris R.P., Booth R.S., 1983, A&A 124, L4
Dickel H.R., Auer L.H. , 1994, ApJ 437, 222
Elitzur M., Goldreich P., Scoville N., 1978, ApJ 205,348
Elitzur M., 1992, "Astronomical masers", Kluwer
Epchtein N., Guibert J., Nguyen-Q-Rieu, Turon P., Wamsteker W., 1980, A&A 85, L1
Evans N.J., Beckwith S., 1977, ApJ 217, 729
Giguere P.T., Woolf N.J., Webber J.C., 1976, ApJ 207, L195
Hrivnak B.J., Kwok S., Volk K.M., 1989, ApJ 346, 265
Jones T.W., Merrill K.M., 1976, ApJ 209, 509
Lang K.R., 1991, "Astrophysical Data. Planets and Stars", Springer
Le Bertre T., Epchtein N., Gispert R., Nguyen-Q-Rieu, Truong-Bach, 1984, A&A 132, 75
Le Sidaner P., Le Bertre T., 1993, A&A 278, 167
Lopez B., Tessier E., Cruzalèbes P., Lefèvre J., Le Bertre T., 1997, A&A 322, 868
Mutel R.L., Fix J.D., Benson J.M., Webber J.C., 1979, ApJ 228, 771
Nedoluha G.E., Bower P.F., 1992, ApJ 392, 249
Netzer N., Knapp G.R., 1987, ApJ 323, 734
Nguyen-Q-Rieu, Laury-Micoulaut C., Winnberg A., Schultz G.V., 1979, A&A 75, 351
Offer A.R., Van Hemert M.C., Van Dishoeck E.F., 1994, J.Chem.Phys 100, 362
Oudmaijer R.D., Groenewegen M.A.T., Matthews H.E., Blommaert J.A.D.L., Sahu K.C., 1996, MNRAS 280, 1062
Richards A.M.S., 1997, Ph.D Thesis, University of Manchester
Skinner C.J., Smith H.A., Sturn E., Barlow M.J., Cohen R.J., Stacey G.J., 1997, Nat 386, 472
Spaans M., van Langevelde H.J., 1992, MNRAS 259, 159
Sylvester R.J. et al. 1997, MNRAS 291, L42
Volk K.M., Kwok S., 1988, ApJ 331, 435
Weaver H., Williams D.R.W., Dieter N.H., Lum W.T., 1965, Nat 208, 29
Zell P.J., Fix J.D., 1990, AJ 99, 314

This article was processed by the author using Springer-Verlag LaTeX A&A style file *L-AA* version 3.